

Coherent oscillations of electrons in tunnel-coupled wells under ultrafast intersubband excitation

A. Hernandez-Cabrera and P. Acoituno

Dpto. Física Basica.

Universidad de La Laguna. La Laguna. 38206-Tenerife. Spain

F.T. Vasko^y

NMRC, University College Cork, Lee Maltings

Prospect Row, Cork, Ireland

and

Institute of Semiconductor Physics, NAS Ukraine

Prospekt Nauki 45, Kiev, 03650, Ukraine

(dated: March 22, 2022)

Ultrafast intersubband excitation of electrons in tunnel-coupled wells is studied depending on the structure parameters, the duration of the infrared pump and the detuning frequency. The temporal dependencies of the photoinduced concentration and dipole moment are obtained for two cases of transitions: from the single ground state to the tunnel-coupled excited states and from the tunnel-coupled states to the single excited state. The peculiarities of dephasing and population relaxation processes are also taken into account. The nonlinear regime of the response is also considered when the splitting energy between the tunnel-coupled levels is renormalized by the photoexcited electron concentration. The dependencies of the period and the amplitude of oscillations on the excitation pulse are presented with a description of the nonlinear oscillations damping.

PACS numbers: 73.40.Gk, 78.47.+p

I. INTRODUCTION

The coherent dynamics of electrons in heterostructures have been thoroughly examined during the past decade for the case of the interband ultrafast excitation by a near-infrared (IR) pulse (see Ref. 1 for review). Recently, a mid-IR pump have been also employed for the treatment of the coherent dynamics of electrons under the intersubband excitation². For example, a coherent transfer of electrons between tunnel-uncoupled states of a double quantum well (DQW) to the common excited state under mid-IR pump was considered in Ref. 3. Moreover, a new type of semiconductor unipolar laser operating in the mid-infrared spectral region was demonstrated. This type of device is based on a three-bound-state coupled DQW with a single-excited level and two coupled lower levels⁴. Thus, an investigation of the coherent dynamics in the tunnel-coupled DQWs under ultrafast mid-IR pump is now appropriate. In the present work we carry out the theory of the ultrafast response on the intersubband excitation between the tunnel-coupled states and the single level, which can be ground or excited.

The study we will fulfill next is based on the quantum kinetic equation for the density matrix averaged over the pump frequency (see evaluation in Ref. 5,6). We will discuss the effects of the intersubband transition peculiarities by means of the intersubband generation rate. With this purpose we take into account the peculiarities of the intersubband excitation for two cases: (A) when the electron transition occurs between the single-ground and the tunnel-coupled excited states, or (B) when the transition takes place from the tunnel-coupled states to the single-excited state. To illustrate these scenarios we have represented in Fig.1 the band diagrams and the dispersion laws for two DQW samples of GaAs-Al_{0.35}Ga_{0.65}As/GaAs, with the layer widths of 150/130/40 Å and 150/20/120 Å, corresponding to the cases (A) and (B), respectively. We have chosen the DQW structures in such a way that the energy separation between the coupled sub-levels, ϵ_{\pm} , is about 10 meV for both cases. In this context the population relaxation is controlled by the LO phonon emission⁷, while the dephasing of the tunnel-coupled states for the case (B) is determined by the quasi-elastic scattering. Since the interwell re-distribution of the charge appears under a relatively low pump intensity, we have considered both the second order response and the nonlinear regime of oscillations. Moreover, we will compare the present results with the corresponding ones to the interband excitation case.

The paper is organized as follows. In Sec. II we derive the balance equations, which describe the coherent response of electrons in DQWs under the ultrafast intersubband excitation. In Sec. III we discuss the emerging quantum beats and the peculiarities of the coherent response under the finite duration excitation, stressing the differences between the cases of intersubband and interband excitation. Sec. IV contains the description of the nonlinear response. The conclusions and discussion of the approximations used are done in the last section.

II. BALANCE EQUATIONS

The coherent dynamics of the electrons, when photoexcited by an ultra-short pulse, is described below in the framework of the second order response on the intersubband excitation. Performing the average over the period of the radiation we obtain the quantum kinetic equation for the density matrix, $\hat{\rho}_t$, in the following form (see Refs. 5,6):

$$\frac{\partial \hat{\rho}_t}{\partial t} + \frac{i}{\hbar} [\hat{H}; \hat{\rho}_t] = \hat{G}_t + \hat{I}_{sc}; \quad (1)$$

where \hat{H} is the Hamiltonian of the DQWs under consideration, \hat{I}_{sc} is the collision integral, and \hat{G}_t is the intersubband generation rate. When the electrons are excited by a transverse electric field $E_z \exp(-i\omega t) + c.c.$, with a frequency ω and a form-factor w_t , the generation rate is given by

$$\hat{G}_t = \frac{1}{\hbar^2} \sum_0 \int d\mathbf{r} \exp(-i\mathbf{r} \cdot \mathbf{p}) \exp(i\mathbf{r} \cdot \mathbf{p}') \hat{\rho}_{eq}^{-1} \exp(i\mathbf{r} \cdot \mathbf{p}) \hat{\rho}_{t+} + H.c. \quad (2)$$

Here $\mathbf{p} \neq 0$, the perturbation operator, $\hat{\rho}_{t+} = (i\hbar^{-1})E_z \hat{v}_z w_t$, is written through the transverse velocity operator \hat{v}_z and $\hat{\rho}_{eq}$ is the equilibrium density matrix when the second-order contributions to the response are taken into account.

Neglecting the non-resonant mixing between the single and the tunnel-coupled levels we describe the system by the scalar distribution function, $F_{pt}^{(k)}$, where $k = 0$; ex correspond to the single electron state [ground] or excited [ex] state for the cases (A) or (B), respectively], and by the 2×2 matrix function \hat{f}_{pt} which describes the tunnel-coupled states $|u\rangle$ and $|l\rangle$ (upper and lower, respectively). Within the framework of the momentum representation, with the in-plane momentum \mathbf{p} , Eq. (1) is transformed into:

$$\begin{aligned} \frac{\partial F_{pt}^{(k)}}{\partial t} &= G_{pt}^{(k)} + I_{sc}^{(k)}(F_{pt}); \\ \frac{\partial \hat{f}_{pt}}{\partial t} + \frac{i}{\hbar} [\hat{h}_{DQW}; \hat{f}_{pt}] &= \hat{G}_{pt} + \hat{I}_{sc}(\hat{f}_{pt}); \end{aligned} \quad (3)$$

where $\hat{h}_{DQW} = (\hbar^{-1})\epsilon_z + T\epsilon_x$ is the matrix Hamiltonian of the tunnel-coupled states, ϵ_z is the interlevel splitting energy, T is the tunnel matrix element, and $\epsilon_{x,z}$ are the Pauli matrices. Here the generation rates are different for the cases (A) and (B). Neglecting the overlap between $|k\rangle$ and $|l\rangle$ states, when $\hbar\omega \neq \epsilon_z$, and doing the straightforward calculations of Eq. (2), we obtain for the case (A):

$$\begin{aligned} G_{pt}^{(0)} &= (F_p - F_p) \frac{eE_z}{\hbar^2} \sum_0 \int d\mathbf{r} w_t \exp(-i\mathbf{r} \cdot \mathbf{p}) \exp(i\mathbf{r} \cdot \mathbf{p}') \\ &\quad \exp(i\mathbf{r} \cdot \mathbf{p}) \exp(-i\mathbf{r} \cdot \mathbf{p}') + H.c.; \\ G_{pt}^{(ex)} &= \frac{eE_z}{\hbar^2} \sum_0 \int d\mathbf{r} w_t \exp(-i\mathbf{r} \cdot \mathbf{p}) \exp(i\mathbf{r} \cdot \mathbf{p}') \\ &\quad \exp(i\mathbf{r} \cdot \mathbf{p}) \exp(-i\mathbf{r} \cdot \mathbf{p}') + H.c.; \end{aligned} \quad (4)$$

where $(F_p - F_p)$ is the ground state equilibrium distribution for the zero temperature case, F_p is the Fermi energy, and $F_p = p^2/2m$ is the kinetic energy with the effective mass. The dephasing time, τ , is introduced here instead of the γ -parameter of Eq. (2) with the aim of describing a finite broadening of the intersubband transitions. For the case (B) we use $\hbar\omega \neq \epsilon_z$ and the generation rate takes form:

$$\begin{aligned} G_{pt}^{(ex)} &= \frac{eE_z}{\hbar^2} \sum_0 \int d\mathbf{r} w_t \exp(-i\mathbf{r} \cdot \mathbf{p}) \exp(i\mathbf{r} \cdot \mathbf{p}') \\ &\quad \exp(i\mathbf{r} \cdot \mathbf{p}) \exp(-i\mathbf{r} \cdot \mathbf{p}') + H.c.; \\ G_{pt}^{(ex)} &= \frac{eE_z}{\hbar^2} \sum_0 \int d\mathbf{r} w_t \exp(-i\mathbf{r} \cdot \mathbf{p}) \exp(i\mathbf{r} \cdot \mathbf{p}') \\ &\quad \exp(i\mathbf{r} \cdot \mathbf{p}) \exp(-i\mathbf{r} \cdot \mathbf{p}') + H.c.; \end{aligned} \quad (5)$$

where $\hat{\rho}_{DQW}$ is the equilibrium density matrix of the tunnel-coupled levels. The detuning frequency in Eqs. (4,5), $\omega - \epsilon_z$, is evaluated through the energy difference between single and tunnel-coupled levels, ϵ_0 (see Fig.1). The remaining matrix elements in Eqs. (4,5) are calculated by using the matrix equalities:

$$\begin{aligned} \exp(i\hat{h}_{DQW} \tau) &= \cos \tau \epsilon_z + i \frac{\epsilon_z + 2T\epsilon_x}{T} \sin \tau \epsilon_x; \\ \hat{\rho}_{DQW} &= f_n^{(+)} + \frac{\epsilon_z + 2T\epsilon_x}{T} f_n^{(-)}; \end{aligned} \quad (6)$$

Here $\tau = \tau^{-1}$ is the frequency of oscillations due to transitions between tunnel-coupled levels, $\tau = \frac{p}{2 + (2T)^2}$ and $f^{(\pm)} = [(\mu_F - \mu = 2) - (\mu_F - \mu + 2)] = 2$.

When doing the summation over the 2D momenta we introduce the population of the single level, $N_t = (2=L^2) \int F_{pt}$, and the 2×2 matrix of concentration $(2=L^2) \int F_{pt} = n_t + (n_t \hat{t})$; which is written through the scalar and vector components of the concentration, n_t and n_t . Due to the particle conservation law, $N_t + n_t = n_{2D}$ with the total 2D concentration n_{2D} , the system (3) is transformed into the balance equations:

$$\frac{dn_t}{dt} = \frac{dN_t}{dt} = G(t) - S(t); \quad \frac{dn_t}{dt} [L \cdot n_t] + (t) = G(t); \quad (7)$$

where $S(t) = n_t^{-1}$ for the case (A) or $S(t) = n_t^{-1}$ for the case (B) and $n_t^{-1} = n_t + n_t^z$. The vector (t) is defined as $(t) = (0; 0; n_t^{-1})$ [case (A)] or $(t) = \hat{n}_t$ [case (B)]. Here n_t^{-1} stands for the population relaxation time between single level and tunnel-coupled states, while the vector $L = (2T^{-1}; 0; -)$ describes the dynamic properties of the tunnel-coupled electronic states. The relaxation matrix in the case (B); \hat{t} is determined by the non-zero components $(\hat{t})_{xx} = (\hat{t})_{yy} = 0^{-1}$, where the dephasing relaxation time, τ_0 , was introduced in Ref. 9 for the case of elastic scattering in DQWs. The generation rates $G(t)$ and $G(t) = [G_x(t); G_y(t); G(t)]$ are obtained from Eqs. (4-6) in the form:

$$G_x(t) = \frac{2T N w_t}{\tau} \int_0^Z \frac{d}{dt} w_{t+} e^{-z} \cos(\omega t + \tau = 2) \quad a_+ \quad \cos(\omega t + \tau = 2) \quad a \quad \cos(\omega t + \tau = 2) \quad ;$$

$$G_y(t) = \frac{2T N w_t}{\tau} \int_0^Z \frac{d}{dt} w_{t+} e^{-z} \sin(\omega t + \tau = 2) \quad a_+ \quad \sin(\omega t + \tau = 2) \quad a \quad \sin(\omega t + \tau = 2) \quad ; \quad (8)$$

$$G(t) = \frac{N w_t}{\tau} \int_0^Z \frac{d}{dt} w_{t+} e^{-z} [a_+ \cos(\omega t + \tau = 2) + b \cos(\omega t + \tau = 2)]; \quad (9)$$

The photoinduced concentration in Eqs. (8,9) is determined as:

$$N = \frac{n_{2D}}{2} \frac{eE_z v_p}{\hbar \omega}^2 \quad (10)$$

with the characteristic pulse duration τ_p and the characteristic velocities v_p^2 equal to $\hbar \omega_j^2$, $\hbar \omega_j^2$ or $\hbar \omega_j^2$, $\hbar \omega_j^2$ for the cases (A) or (B); respectively. The coefficients a in Eq. (8) are given by: $a = (1 - n = n_{2D}) = 2$ [in moreover $n = 0$ for the DQW (A)] while, in Eq. (9), $b = 1 - \tau$ for the case (A) and $b = (1 - \tau)(1 - n = n_{2D}) = 2$ for the DQW (B), where $n = n_{2D} - \tau$.

Next, taking into account the Coulomb renormalization of the tunnel-coupled levels, we have to replace \hat{n}_{DQW} in the matrix equation (3) by the Hartree-Fock Hamiltonian, \hat{n}_{DQW} , written in the form (see Refs. 10 and 11):

$$\hat{n}_{DQW} = \hat{n}_{DQW} + \sum_Q v_Q n_{Qt} e^{iQ \cdot r} e^{iQ \cdot r} \hat{t} e^{iQ \cdot r} \quad (11)$$

Here Q is the 3D wave vector, v_Q is the Coulomb matrix element, and $n_{Qt} = \text{Tr}(\hat{t} e^{iQ \cdot r})$ is the Fourier transform of the electron density. Further transformations lead to the balance equation (7) with the renormalized vector L_t written through the level splitting energy

$$(t) = \frac{4 e^2}{Z} Z (n_t^z - n_t); \quad (12)$$

where Z is the distance between the centers of l- and r-QWs and ϵ is the dielectric permittivity supposed to be uniform across the DQWs. The signs + and - in Eq. (12) correspond to the cases (A) and (B); respectively. The evaluation of (t) coincides with that done for the DQW (A) in Ref. 10.

III. QUANTUM BEATS

In this section we present a solution of the linear system of balance equations (7), neglecting the second addendum in Eq. (12), for the cases of short and finite pulse duration. Respecting the short-pulse approximation, if the pulse duration $\tau_p \ll \tau^{-1}$; τ^{-1} , the generation rates [Eqs. (8) and (9)] take the forms: $G_x(t) \approx a (2T = \tau) N_p(t)$,

$G_y(t) \neq 0$, and $G(t) \neq b_+ N_p(t)$ with the δ -like function: $n_p(t) = (2w_t)^{R_0} \int_0^t dt' w_{t'} = \frac{2}{R_0} \int_0^t dt' w_{t'}^2$. Thus, the photoinduced redistribution of the concentration can be written as the step-like function: $n_t = b_+ N \int_0^t dt' w_{t'}^2$ which is proportional to the step function $w(t)$ if $w \neq 0$. Since the photoinduced dipole moment is expressed through n_t^z , we obtain the z-component of n_t in the form:

$$n_t^z = (t)N \cos \frac{\tau}{2}(t - p) + \cos(\tau t) \quad (13)$$

For the short-pulse approximation, the differences between the above-presented results and those corresponding to the case of the interband excitation (as considered in Ref. 5) are mainly attributable to the different characteristic concentrations and to the strong damping caused by the interband relaxation. Comparing Eq. (10) with the characteristic concentration for the interband excitation, N [given by the Eq. (18) in Ref. 5], we obtain

$$\frac{N}{N} \sim \frac{4n_{2D}}{2D} \sim \frac{E_2 v_2 n_g^2}{E P n_o^2}; \quad (14)$$

where the interband excitation is characterized by the Kane velocity P , the gap n_g , the reduced density of states n_{2D} , and the field strength E . If $E_2 = E$, and the pulse is not too short ($p = 1$ ps), the ratio (14) is about 16 [case (A)] and 26 [case (B)] for the GaAlAs-based structures with a total 2D-concentration $n_{2D} \sim 1.4 \cdot 10^{11} \text{ cm}^{-2}$ and the dimensions used in Fig. 1. Thus, the intersubband excitation appears to be more effective than the interband one.

The response seems to be more complicated for the finite pulse duration case due to the peculiarities of the relaxation processes. We have used below the Gaussian form-factor, $w_t = \exp[-(t-p)^2/2]$, a semiempirical value of the damping $\gamma_0 = 35 \text{ ps}^{-1}$, a dephasing time caused by the finite broadening of the intersubband transition $\tau_2 = 1 \text{ ps}^{13,14}$ and an interband relaxation time due to LO phonons $\tau_1 = 3.5 \text{ ps}^{4,14}$. We consider first the evolution of the concentration. Fig. 2 shows the evolution of n_t with the increase of the pulse duration $p/\tau = 2$, for three detuning frequencies $\Delta = 0$, $\Delta = \tau = 2$, and $\Delta = \tau$ [Figs. 2(a-c), respectively] and for the DQW (A). For DQW (B) the only difference is that the amplitude of the concentration n_t is half of the corresponding to the structure (A) because, initially, there are two occupied levels in DQW (B). Therefore, we will pass by its interpretation, restricting ourselves to the case (A). One can see a new non-monotonic behavior in contrast to the one of the interband excitation case⁵. For $0 < p/\tau = 2 < 1$; $n_t = N$ behaves like in the interband case (corresponding to the short pulse context) with some type of oscillations superimposed. For $p/\tau = 2 \gg 1$; $n_t = N$ these oscillations are strongly amplified around $t = 0$ for $\Delta = 0$ and $\Delta = \tau$, when the excited sublevel(s) is(are) not syntonized, before decaying. It should be noted that the excitation pulse is centered at $t = 0$. The number of oscillations depends on the pulse duration p , as Figs. 2(a;c) display. It is important to note that these oscillations have a period $2 = \tau$; twice the n_t^z quantum beats period because such oscillations are controlled by the term $\Delta + \tau = 2$ and strongly influence the initial stages of n_t^z : An exception takes place when one of the levels is syntonized, e.g., $\Delta = \tau = 2$. Then, the concentration shows a monotonic behavior with a growth rate similar to that of the interband pump [Fig. 2(b)]. Also visible in Fig. (2) is the exponential damping of the photoexcited electrons caused by the dephasing time, τ_2 .

Figs. 3 and 4 illustrate temporal evolution of the dipole moment, which is proportional to n_t^z , for different regions of parameters, $p/\tau = \tau$, and Δ . Figs. 3(a), 4(a) stand for the sample (A) and Figs. 3(b), 4(b) for the sample (B), respectively. The main difference between the finite pulse excitation and the short pulse excitation is the existence of two different regimes in the former event. When $\Delta = 0$ and $\tau = 0$ [upper panels of Figs. 3(a;b)] the finite duration pulse produces a transition from a regime in which the electron density is mainly located in a well to two-well oscillations. This transition occurs when the pulse is switched on. The dipole moment exhibits the biggest oscillation amplitude while the pulse holds, then decaying due to relaxation until reaching the equilibrium after switching off the pulse. The balance situation is different for the two samples studied. In the first one the electronic redistribution between both wells are quickly reached, because the photoexcited electrons of the coupled levels decay to the ground state by means of the LO phonon emission. We must keep in mind that we are representing here the distribution n_t^z corresponding to the coupled excited levels. On the contrary, in the second sample, (B); one can see the non-excited coupled levels. For this reason, the oscillations stay during some time until the electronic balance redistribution between the wells is reached because of the inter-subband dephasing relaxation. The time τ_0 for the last process is longer than that for the interband relaxation, τ_1 (see numerical values above). Figs. 3 and 4 show these features of the dipole moment in the cases of zero-phase shift ($\tau/p = 4$) and π -phase shift ($\tau/p = 5$) as indicated in figure captions. Fig. 3 has been calculated for $\tau = 0$, when the two tunnel-coupled states resonate and it corresponds to applied electric fields of 7 kV/cm (DQW (A)) and 2 kV/cm (DQW (B)), respectively. Fig. 4 has been calculated for $\tau = 0.7$, out of the resonance of the tunnel-coupled levels. In this situation the electronic concentration mainly occupies the left well and the oscillation amplitude becomes quenched.

The influence of the detuning frequency when $\tau = 0$ can be explained as follows. If $\Delta = 0$ (upper panel of Fig. 3), a fast transfer of the electron density from the well in which electrons were initially created to the other well occurs.

For $\delta = \delta_T = 2$ (lower panel of Figs. 3), the electron density oscillates between coupled levels from the beginning of the excitation. Out of the resonance between the tunnel-coupled levels ($\delta \neq 0$, Fig. 4) most of the electron density remains in the left well and the transfer doesn't become effective because of level decoupling. It is specially striking the practical disappearance of the oscillations when $\delta = \delta_T = 2$.

IV. NONLINEAR COHERENT RESPONSE

Now we turn to the description of the nonlinear response. In order to do this we will take into account the Coulomb renormalization of the level splitting energy, when n_t is governed by the nonlinear system of Eqs. (7), and L_t is determined through Eq. (12). The characteristic concentration, N ; directly related to the pulse excitation density, is responsible for the nonlinearity. In order to get an effective Coulomb renormalization we have used $N \approx 2 \cdot 10^{10} \text{ cm}^{-2}$ (corresponding to an excitation energy density of about $10 \text{ J} \cdot \text{cm}^{-2}$) when the nonlinear response becomes noticeable.

Figs. 5(a;b) show the evolution of the dipole moment, n_t^z ; corresponding to a characteristic concentration of $N = 0.14 n_{2D} (\delta_T = 2)^2$; at the coupled-level resonance ($\delta = 0$), zero-phase shift, and for structures (A) and (B), respectively. We should always keep in mind that N depends on δ_p^2 . Thus, for a fixed excitation energy, we have a different N values for each pulse duration. The main result we can observe is that the oscillation period decreases and this is caused by a high N value. This period also depends on the detuning frequency. As a consequence of this dependency, a slight Coulomb-induced dephasing appears between different δ_p and δ cases. This behavior is more noticeable in the structure (B) than in (A) because of the relation $N e^2 Z = T$, which mainly determines Coulomb effects in Eq. (7) (see Ref. 10), is greater in the former case for the same characteristic concentration because of the different values of V_p . Another feature induced by the Coulomb interaction occurs while the excitation pulse is acting on the samples. The term $\delta + \delta_T = 2$, which initially controls n_t (and dipole moment oscillations), loses part of its importance and the masking of the intersubband oscillations diminishes.

By comparing Fig. 5 with Fig. 3 one can see a slight displacement of the electronic concentration to the left QW caused by the above mentioned Coulomb renormalization when $\delta = 0$ (upper panels). Once again the detuning frequency plays the main role in the oscillatory behavior, leading to a concentration, which is located in the left well, one order of magnitude higher for $\delta = \delta_T = 2$ than for $\delta = 0$. Such a bearing is common for both samples studied.

We have already shown (Fig. 4) that, being out of the resonance condition (e.g. $\delta = 0.7$), differences produced by the detuning frequency are small and this kind of behavior remains when the Coulomb renormalization is introduced [Figs. 6(a;b)]. However, there is a clear dissimilarity between structures (A) and (B). In the first sample the electronic concentration oscillates between the two wells from when the excitation pulse is switched on [Fig. 6(a)]. Such behavior is caused by a new situation of resonance at $\delta \neq 0$. To understand this point we must underline that the δ -values corresponding to resonance and off-resonance are strictly defined for the linear response. When the level renormalization is included resonance conditions vary and, hence, the electric fields to get them will also vary. In the other case, and for the same reason, electrons always prefer to stay mainly in the left QW [Fig. 6(b)]. These different behaviors are caused by the opposite sign in the expression for the Coulomb level splitting renormalization (Eq. 12). Finally, one can observe as a general bearing that the dipole moment oscillations are weak in the structure (A). Furthermore, for both structures, the temporal evolution of the dipole moment loses its oscillatory behavior almost completely when $\delta = \delta_T = 2$, the evolution depending essentially on the total concentration of excited electrons.

V. CONCLUDING REMARKS

Summarizing, we have described the coherent dynamics of electrons in DQWs taking into account the peculiarities of the intersubband excitation and relaxation for transitions between single and tunnel-coupled states. The temporal dependencies of the photoinduced concentration and the dipole moment are obtained both for the second order response and the nonlinear regime, when the splitting energy is renormalized by the photoexcited charge.

Furthermore, we discuss the assumptions made. Both the tight-binding approximation for the description of the tunnel-coupled states and the use of the parabolic dispersion laws are valid for the DQWs under consideration. The simple relaxation time approach is also widely used for the description of similar structures. Applying the single-particle description of the high-frequency response we have neglected the Coulomb renormalization of the intersubband transitions due to depolarization and exchange effects, so that the nonlinear regime of the response under a not very low pump intensity may take place if δ is not very big. On the other hand, we do not consider here the high-intensity pump case restricting ourselves to the inequality $N < n_{2D}$ when there is no Rabi oscillations. All these conditions are satisfied for the concentrations and intensities used in Sects. III and IV.

To conclude, the peculiarities of coherent dynamics under the intersubband transitions of electrons described in sections III and IV are interesting in order to select effective conditions both for the THz emission, observed only under

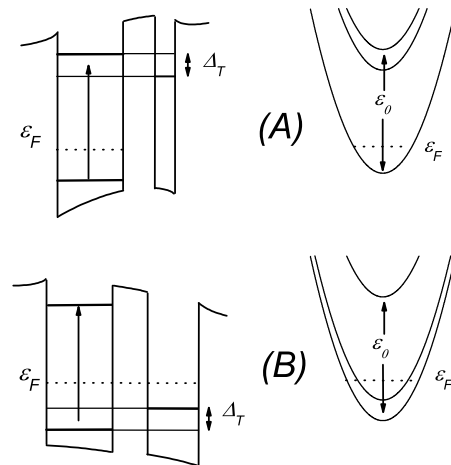


FIG. 1: Band diagrams and dispersion laws for the intersubband excitation of tunnel-coupled wells with single-ground (A) or single-excited (B) states.

the interband excitation, and for the photoinduced concentration redistribution (see recent mid-IR measurements in a single QW¹⁵). It would also be interesting to verify scattering mechanisms by the use of this approach and to study the high-intensity pump, when an interplay between the nonlinear dynamics and Rabi oscillations appears. This case requires a special consideration.

Acknowledgment: This work has been supported in part by Consejería de Educación, Cultura y Deportes, Gobierno Autónomo de Canarias and by Science Foundation Ireland.

Electronic address: jheman@ulles

Electronic address: ftvasko@yahoo.com

- ¹ F. Rossi and T. Kuhn, *Rev. of Mod. Phys.*, **74**, 895 (2002).
- ² T. Elsaesser and M. Woerner 1999, *Phys. Rep.* **321**, 254 (1999).
- ³ P. Tamborenea and H. M. etiu, *Phys. Lett. A* **240** 265, (1998); M. Rufenacht, S. T sujino, S.J. Allen, W. Schoendekel, and P. Petro, *Physica Status Solidi B* **221**, 407 (2000); S. T sujino, M. Rufenacht, P. Miranda, S.J. Allen, P. Tamborenea, W. Schoendekel, G. Herold, G. Lupke, T. Lundstrom, P. Petro, H. M. etiu, and D. Moses, *Physica Status Solidi B* **221**, 391 (2000).
- ⁴ F. H. Julien, O. Gauthier-Lafaye, Ph. Boucaud, S. Sauvage, J-M. Lourtioz, V. Thierry-Mieg, and R. P lanel, in *Intersubband Transitions in Quantum Wells*, S.S. Li and Y-K. Su Eds. Kluwer Academic Pub.. (Boston, 1998); O. Gauthier-Lafaye, S. Sauvage, P. Baucaud, F. H. Julien, R. P razeres, F. G lotin, J-M. Ortega, V. Thierry-Mieg, R. P lanel, J-P. Leburton, and V. Berger, *Appl. Phys. Lett.* **70**, 3197 (1997).
- ⁵ F. T. Vasko, O. E. Raichev, *Phys. Rev. B* **51**, 16965 (1995).
- ⁶ F. T. Vasko and A. Kuznetsov, *Electronic States and Optical Transitions in Semiconductor Heterostructures*. Springer, 1998.
- ⁷ C. Gmachl, F. Capasso, D. L. Sivco, A. Y. Cho, *Reports on Progr. in Phys.* **64**, 1533 (2001).
- ⁸ Note, that the same ϵ_1 appears in the population balance equation and here because we neglect the overlap between ψ_i and ψ_j states.
- ⁹ F. T. Vasko, O. E. Raichev, *JETP* **81**, 1146 (1995).
- ¹⁰ O. E. Raichev, *Phys. Rev. B* **51**, 17713 (1995); O. E. Raichev, F. T. Vasko, A. Hernandez-Cabrera, and P. Aceituno, *Phys. Rev. B* **56**, 4802 (1997).
- ¹¹ F. T. Vasko, *JETP* **93**, 1279 (2001).
- ¹² N. Sekine, K. Hirakawa, and Y. A rakawa, *Jpn. J. Appl. Phys.* **37**, 1643 (1998); F. W olter, H. G. Roskos, P. H. Bolivar, G. Bartels, H. Kurz, K. Kohler, H. T. G rahn, and R. Hey, *Phys. Stat. Solidi B* **204**, 83 (1997).
- ¹³ Y. Lavon, A. Sa'ar, F. Julien, J-P. Leburton, and R. P lanel, in *Intersubband Transitions in Quantum Wells*, S.S. Li and Y-K. Su Eds. Kluwer Academic Pub. (Boston, 1998).
- ¹⁴ T. K. U num a, T. Takahashi, T. Noda, and M. Yoshita, *Appl. Phys. Lett.* **78**, 3448 (2001).
- ¹⁵ M. Woerner, R. A. Kaindl, F. Eickemeyer, K. Reinann, T. Elsaesser, A. M. Weiner, R. Hey, and K. H. Plog, *Physica B* **314**, 244 (2002).

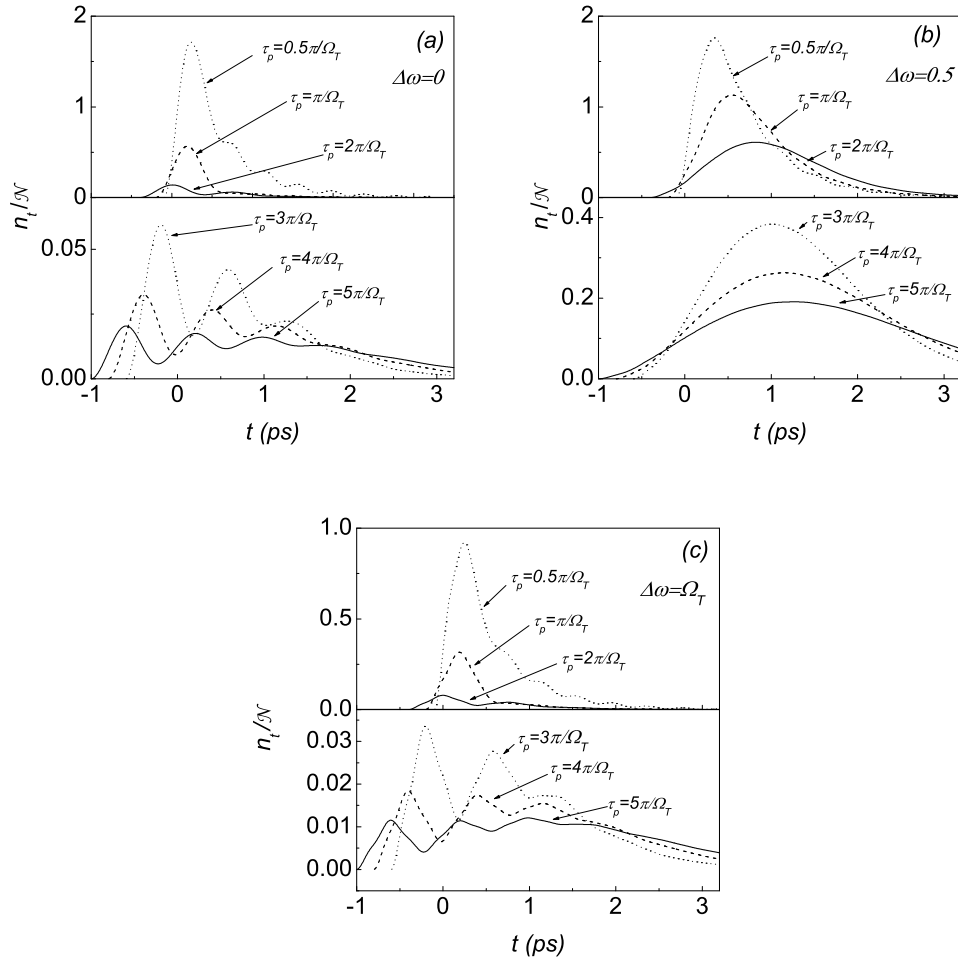


FIG. 2: Temporal evolution of the excited electrons concentration n_t^z for different pulse duration values and for the structure (A). Pulse duration times are indicated by arrows and $\Delta\omega = 0$ (a); $\Delta\omega = \Omega_T/2$ (b); $\Delta\omega = \Omega_T$ (c).

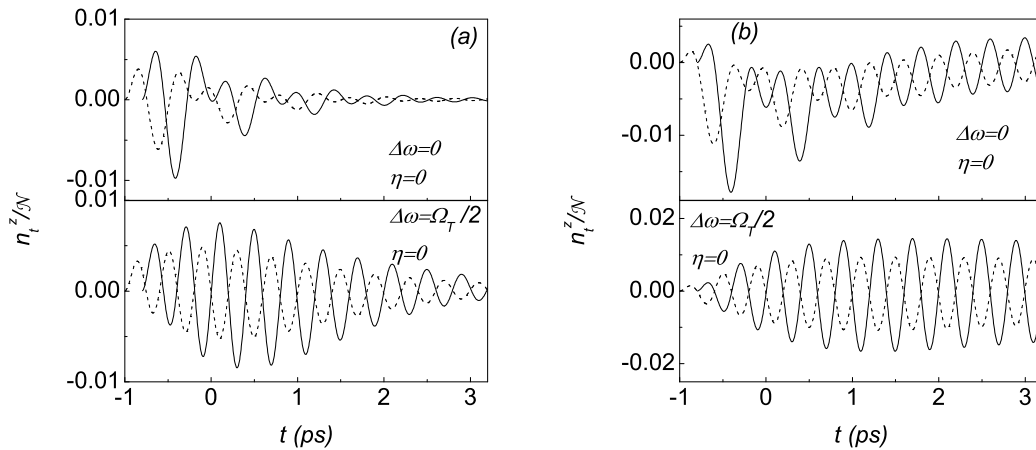


FIG. 3: Temporal evolution of n_t^z/N for $\Delta\omega = 0..$ Figures 3a and 3b correspond to structures (A) and (B), respectively. Solid and dashed curves are plotted for $\tau_p = 1.76$ ps (zero-phase shift) and for $\tau_p = 2.2$ ps (π -phase shift). Upper and lower panels correspond to $\Delta\omega = 0$ and $\Delta\omega = \Omega_T/2$.

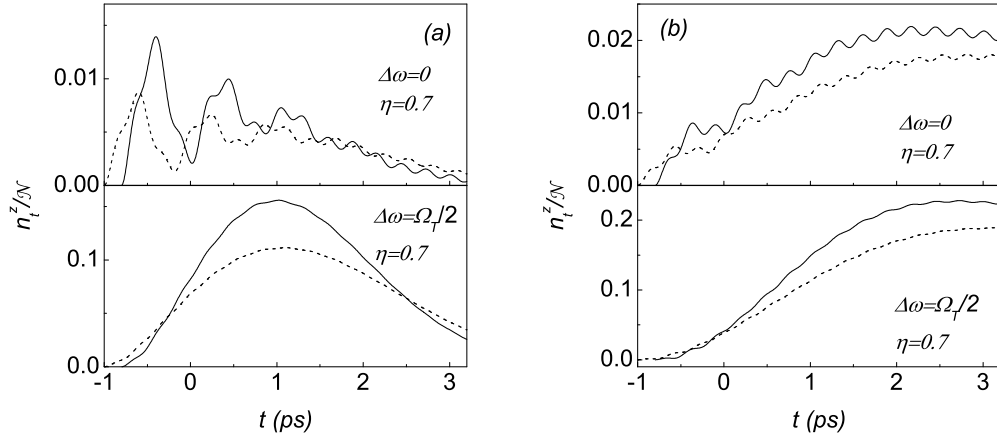


FIG. 4: The same as in Fig. 3 for $\eta = 0.7$. Solid line: $p = 1.76$ ps.

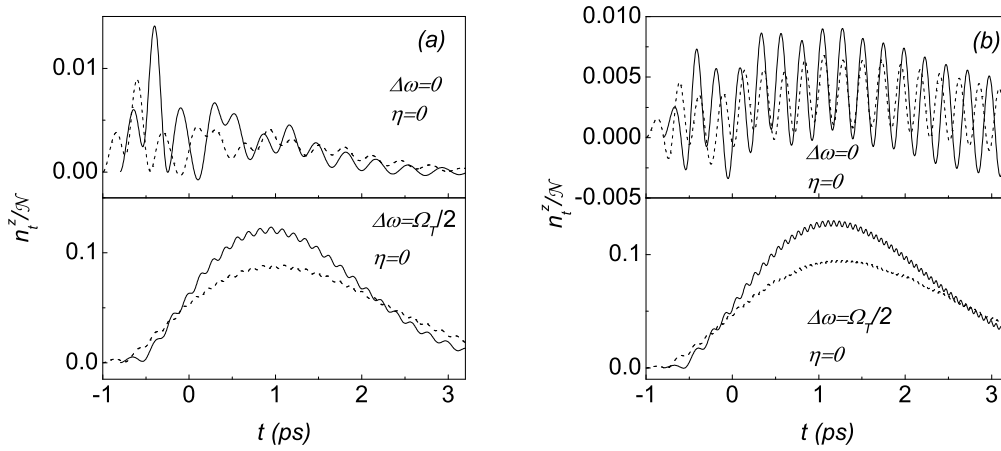


FIG. 5: Nonlinear regime of the dipole moment n_t^z/N for $\eta = 0$. Figures 5a and 5b correspond to DQWs (A) and (B), respectively. Solid and dashed curves are plotted for $p = 1.76$ ps (zero-phase shift) and for $p = 2.2$ ps (π -phase shift). Upper and lower panels correspond to $\Delta\omega = 0$ and $\Delta\omega = \Omega_r/2$.

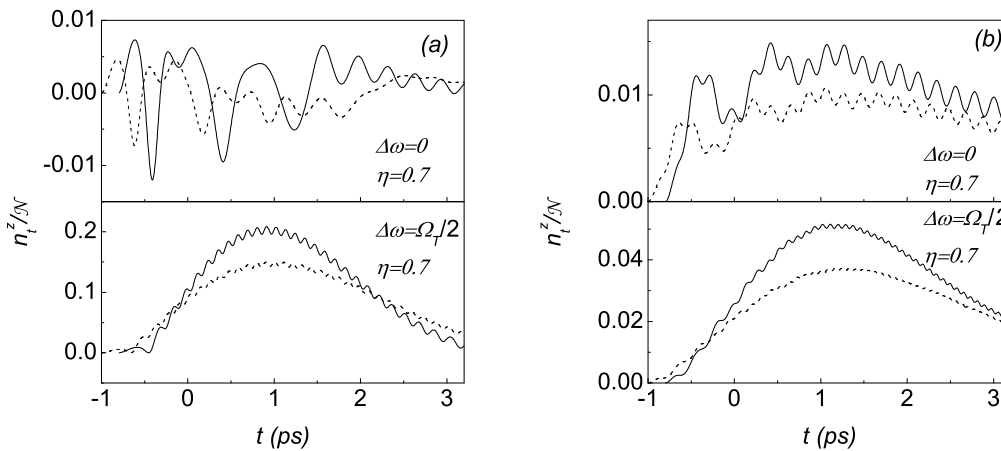


FIG. 6: The same as Fig. 5 for $\eta = 0.7$.